Nuclear Inst. and Methods in Physics Research, A 871 (2017) 135–141

Contents lists available at ScienceDirect

Nuclear Inst. and Methods in Physics Research, A

journal homepage: www.elsevier.com/locate/nima

Direct neutron-multiplicity sorting with a flat-efficiency detector

Hiroaki Utsunomiya [a,*], Ioana Gheorghe [b,c], Dan M. Filipescu [b], Tudor Glodariu [b], Sergey Belyshev [d], Konstantin Stopani [d], Vladimir Varlamov [d], Boris Ishkhanov [d], Seitarou Katayama [a], Daiki Takenaka [a], Takashi Ari-izumi [a], Sho Amano [e], Shuji Miyamoto [e]

[a] Department of Physics, Konan University, Okamoto 8-9-1, Higashinada, Kobe 658-8501, Japan
[b] ELI-NP, "Horia Hulubei" National Institute for Physics and Nuclear Engineering (IFIN-HH), 30 Reactorului, 077125 Bucharest-Magurele, Romania
[c] Faculty of Physics, University of Bucharest, RO-077125, Bucharest, Romania
[d] Lomonosov Moscow State University, Skobeltsyn Institute of Nuclear Physics, 119991 Moscow, Russia
[e] Laboratory of Advanced Science and Technology for Industry, University of Hyogo, 3-1-2 Kouto, Kamigori, Ako-gun, Hyogo, 678-1205, Japan

ARTICLE INFO

Keywords:
Neutron-multiplicity sorting
Flat-efficiency neutron detector
Partial photoneutron cross sections

ABSTRACT

A novel technique of direct neutron-multiplicity sorting with a flat-efficiency detector is proposed to resolve the long-standing discrepancy between the Livermore and Saclay data of partial photoneutron cross sections. A flat-response neutron detector with the detection efficiency of 36.5 ± 1.6% over a neutron energy range 0.01–5.0 MeV was developed by optimizing triple-ring configurations of He proportional counters embedded in a polyethylene moderator. The technique forms a foundation of measuring cross sections with $x = 1 - 3$ for the photonuclear data project of the International Atomic Energy Agency. The methodology of direct neutron-multiplicity sorting and key experimental elements are presented.

© 2017 Elsevier B.V. All rights reserved.

1. Introduction

The majority of photoneutron cross sections were obtained using quasimonochromatic photon beams produced in positron annihilation in flight at the two national facilities of the Lawrence Livermore National Laboratory (USA) and Centre d'Etudes Nucleaires de Saclay (France) during 1950s through 1980s for a systematic understanding of the isovector giant dipole resonance [1]. The ATLAS of photoneutron cross sections was published in 1988 [2] summarizing the accumulated data followed by the publication of the IAEA-TECDOC-1178 in 2000 [3], the compilation and evaluation of photonuclear data for 164 isotopes of 48 elements from ^{2}H to ^{241}Pu. Large discrepancies in partial photoneutron cross sections as well as in (γ, n) cross sections below two-neutron separation energies are well-recognized [4,5]; In many cases of partial cross sections, the Saclay provided larger cross sections for (γ, n) reactions than the Livermore and vice versa for $(\gamma, 2n)$ reactions. It was shown [6] that the ratio of the Saclay data to the Livermore data of integrated total cross sections, $R^{int} = \sigma_S^{int}/\sigma_L^{int}$, varies from 0.65 to 1.35 over 19 nuclei from ^{51}V to ^{238}U and that the ratio between the Saclay and Livermore data of integrated partial cross sections, when averaged over the 19 nuclei, is very different for the $(\gamma, 1n)$ and $(\gamma, 2n)$ reactions: $\langle R^{int}(1n)\rangle \approx 1.08$ and $\langle R^{int}(2n)\rangle \approx 0.83$. Elaborate efforts of the evaluation including those based on the transitional neutron-multiplicity function (F) [6] have also shown that the discrepancies cannot be resolved in a systematic way. This fact led to launching a new Coordinated Research Project (CRP) by the International Atomic Energy Agency (IAEA) to update the photonuclear data library, IAEA-TECDOC-1178.

There may be two factors of uncertainties in the past data obtained at Livermore and Saclay: one is related to the γ-ray source commonly used, while the other the detection methods separately used. The quasimonochromatic γ-ray beam produced in positron annihilation in flight was accompanied by strong positron bremsstrahlung produced in passing the γ-ray production target (Be), which formed background γ rays. The subtraction of the background contribution to the production of photoneutrons required the second measurement with electron beams ideally under the same accelerator condition. A complication may have arisen in subtracting a large number from another large number in deducing photoneutron events, especially in the energy region above the peak of the giant dipole resonance (GDR) where cross sections decrease with increasing γ-ray energy. Although this is a common source of uncertainties involved in the Livermore and Saclay data, it may have partly caused the discrepancy under discussions because the accelerator

* Corresponding author.
E-mail address: hiro@konan-u.ac.jp (H. Utsunomiya).

http://dx.doi.org/10.1016/j.nima.2017.08.001
Received 30 March 2017; Received in revised form 20 July 2017; Accepted 1 August 2017
Available online 6 August 2017
0168-9002/© 2017 Elsevier B.V. All rights reserved.

condition for the production of γ-ray beams was obviously not the same at Livermore and Saclay. Negative (γ, n) cross sections and the resultant F_2 values larger than the upper limit (0.5) reported for many nuclei from ^{63}Cu to ^{209}Bi [7,8] may be attributed to this subtraction procedure.

It is more likely that the discrepancy has arisen from the detection methods employed separately. Both methods are based on direct neutron-multiplicity sorting, but with different detectors: BF_3 counters embedded in a neutron moderator at Livermore [1]; and gadolinium-loaded liquid scintillator at Saclay [9]. In this paper, we focus on neutron-multiplicity sorting with a slow neutron detector of the Livermore type. The Saclay detector with efficiencies more than 90% at neutron energies less than 5 MeV may have suffered from pile-up and background events [1] as well as dead time associated with a γ flash from the target.

2. Direct neutron-multiplicity sorting

The Livermore detectors were large arrays of $^{10}BF_3$ tubes embedded in a paraffin or polyethylene moderator [10–12]. The 4π paraffin-moderated detector consisting of 48 $^{10}BF_3$ tubes [11] had 45%–30% detection efficiencies over neutron energies up to 5 MeV. The ring-ratio (RR) technique [1,11] was used to determine the average neutron energies. However, the RR technique, which is applied to multi-neutron coincidence events, cannot directly determine the average neutron energy for individual (γ, xn) reactions. This may be a source of uncertainties involved in the Livermore data of partial photoneutron cross sections.

2.1. Multi-neutron coincidences vs. partial photoneutron reactions

The number of neutrons, N_x, emitted in the (γ, xn) reactions with the neutron-multiplicity x ($x = 1, 2, 3, \ldots$) is expressed by

$$N_x = N_\gamma \cdot N_T \cdot \sigma(\gamma, xn), \tag{1}$$

where N_γ is the number of γ-rays incident on a target; N_T is the number of target nuclei per unit area; and $\sigma(\gamma, xn)$ is the partial photoneutron cross section.

Let us consider a multi-neutron coincidence measurement for (γ, xn) cross sections using a neutron detector with an efficiency ε. We experimentally separate j-fold neutron-coincidence events for single ($j = 1$), double ($j = 2$), triple ($j = 3$), …, and n-fold neutron coincidences, respectively, where n is the maximum neutron multiplicity. The number of j-fold events, N_j, is given by

$$N_j = \sum_{x=j}^{n} {}_xC_j \cdot N_x \cdot \varepsilon(E_x)^j \cdot (1 - \varepsilon(E_x))^{x-j}. \tag{2}$$

For $n = 3$, single, double, and triple neutron events (N_s, N_s, and N_t), respectively, are expressed explicitly by

$$N_s = N_1 \cdot \varepsilon(E_1) + N_2 \cdot {}_2C_1 \cdot \varepsilon(E_2) \cdot (1 - \varepsilon(E_2)) + N_3 \cdot {}_3C_1 \cdot \varepsilon(E_3) \cdot (1 - \varepsilon(E_3))^2, \tag{3}$$

$$N_d = N_2 \cdot \varepsilon(E_2)^2 + N_3 \cdot {}_3C_2 \cdot \varepsilon(E_3)^2 \cdot (1 - \varepsilon(E_3)), \tag{4}$$

and

$$N_t = N_3 \cdot \varepsilon(E_3)^3. \tag{5}$$

One can see that there are contributions from all possible (γ, xn) reactions to the single neutron events. The second term of Eq. (3), for example, comes from the fact that we detect one neutron out of two neutrons emitted in the $(\gamma, 2n)$ reaction and undetect the other neutron. Note that the efficiency ε, in general, depends on E_x, the kinetic energy of neutrons emitted in the (γ, xn) reaction. Here we do not separate the kinetic energies of two neutrons emitted in the $(\gamma, 2n)$ reaction. However, there must be correlations between the two neutrons; the higher (lower) the kinetic energy of the first neutron, the lower (higher) that of the second neutron. Therefore, we remark that the second term of Eq. (3) is more precisely expressed by $N_2 \cdot \varepsilon(E_{21}) \cdot (1 - \varepsilon(E_{22})) + N_2 \cdot \varepsilon(E_{22}) \cdot (1 - \varepsilon(E_{21}))$, using kinetic energies (E_{21} and E_{22}) of the first neutron and second neutron emitted.

One cannot solve the set of n equations (Eq. (2)) to obtain N_x, from which the partial photoneutron cross section ($\sigma(\gamma, xn)$) in Eq. (1)) is determined, unless neutron kinetic energies are known. Experimentally, the RR technique can be applied to the j-fold neutron events so that the technique cannot directly determine the average neutron kinetic energy for individual (γ, xn) reactions. It is obvious that making the efficiency (ε in Eqs. (3)–(5)) independent of neutron kinetic energies (E_x) is an ideal solution to the direct neutron-multiplicity sorting. Thus, it is essential to develop a flat-response neutron detector over a broad neutron energy range. The degree of the flatness is a source of the systematic uncertainty in determining partial photoneutron cross sections.

2.2. Flat-efficiency neutron detector

Besides a flat response to neutron energies, we also need to pursue a high efficiency for neutron coincidence measurements because the efficiency of detecting j neutrons in coincidences (ε^j) limits the detectable maximum neutron-multiplicity. A long counter developed by East and Walton [13] consisting of five ^{3}He counters embedded in a polyethylene cylinder has a flat response over the neutron energy range of 30 keV–5 MeV with an intrinsic efficiency 11.5%. The intrinsic efficiency around 10%, which is equal to the total detection efficiency when 100% of the 4π solid angle is geometrically covered by the detector, is however not sufficient because the detection efficiency for two neutrons in coincidences goes down to ~1%. Previously we developed a high-efficiency neutron detector consisting of 20 ^{3}He counters embedded in a triple-ring configuration in a polyethylene cube for (γ, n) cross section measurements below two-neutron separation energies [14]. This detector is featured with high-efficiencies more than 60% for neutron energies below 1 MeV, but has a strong neutron-energy dependence.

We have developed a flat-response neutron detector by modifying the triple-ring configuration of the high-efficiency neutron detector. The flat response was achieved by weakening the strong-energy dependence of the inner ring (R1), which shows a rapid decrease with increasing neutron energy, at the cost of the large detection efficiency and compensating the energy dependence with increasing efficiencies of the middle (R2) and outer (R3) rings. The numbers of ^{3}He counters and the distances of the three rings were optimized by Monte Carlo simulations with the MCNP code [15].

The flat-efficiency neutron detector (FED) consists of three concentric rings of 4, 9, and 18 ^{3}He counters embedded in a 46 cm (horizontally) × 46 cm (vertically) × 50 cm (along the beam axis) polyethylene moderator at the distances of 5.5, 13.0 and 16.0 cm from the γ-ray beam axis, respectively. The ^{3}He counters are cylindrically shaped with a 2.5 cm diameter and 45 cm-long active volume (total length of 55 cm). The counters contain a 10 atm gas mixture of ^{3}He with 87.2% atomic fraction (100% isotopic fraction) and CO_2. The moderator is shielded by additional 5 cm-thick borated polyethylene plates for background neutron suppression. Figs. 1 and 2 show the geometrical configuration of 31 ^{3}He counters in the polyethylene moderator and a photograph of the flat-response detector, respectively.

The efficiency of the FED was calibrated with a ^{252}Cf source whose absolute emission rate was determined to be $(1.62 \pm 0.04) \times 10^4$ neutrons per second at the National Metrology Institute of Japan. Fig. 3 shows the results of the calibration in comparison with the MCNP Monte Carlo simulations. The total efficiency summed over the three rings is 37.3 ± 0.8% at 2.13 MeV, the average energy ($\bar{E} = 3T/2$) of the ^{252}Cf neutron spectrum corresponding to the temperature $T = 1.42$ MeV [16], where the fission spectrum is given by the Maxwell–Boltzmann distribution, $P(E) \propto E^{1/2} \cdot \exp(-E/T)$. The Monte Carlo simulations were performed for both monochromatic neutrons and neutron-evaporation

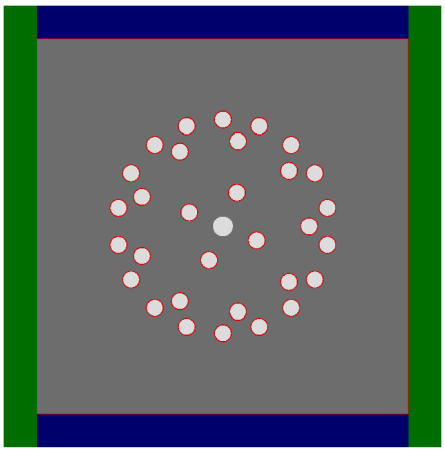

Fig. 1. (Color online) The layout of triple rings of ^{3}He counters for the flat-response neutron detector.

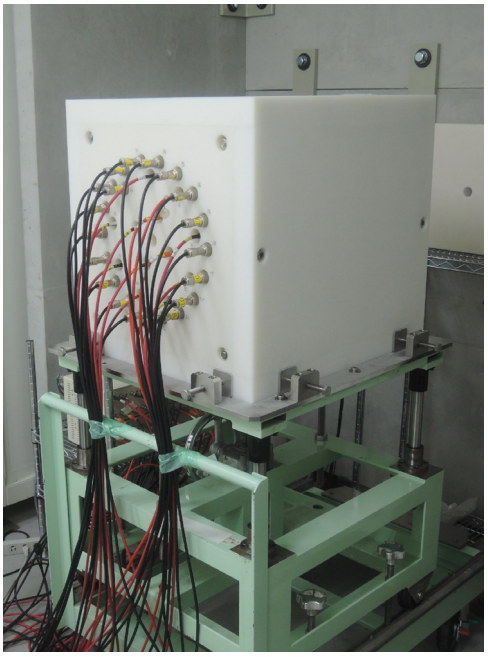

Fig. 2. (Color online) The experimental setup of the flat-response neutron detector.

spectra expressed by $P(E) \propto E \cdot \exp(-E/T)$ with the Weisskopf–Ewing model [17]. Results for the evaporation spectra are shown at the average neutron energy ($\bar{E} = 2T$) in Fig. 3. Naturally the results of the calibration are better reproduced by the simulations for evaporation spectra. The total efficiency changes from 37.8% (38.1%) at 10 keV to 32.9% (33.1%) at 5.0 MeV for evaporation spectra (monochromatic neutrons). The total efficiency averaged over neutron energies up to 3, 4, 5, 6, and 7 MeV is 37.3 ± 0.69, 36.7 ± 1.1, 36.5 ± 1.6, 35.9 ± 2.1, and 35.2 ± 2.2% (37.7 ± 0.46, 37.4 ± 0.77, 36.8 ± 1.4, 36.0 ± 2.1, and 35.3 ± 2.8%), respectively, for evaporation spectra (monochromatic neutrons). The uncertainty represents one standard deviation.

Fig. 4 shows results of Monte Carlo statistical model calculations of energy spectra for successive neutron emissions in the ^{209}Bi(γ, xn) reaction for $x = 2$, 3, 4, and 5 at 40 MeV [18]. At this energy, the most dominant reaction channel is $(\gamma, 4n)$ with 95.1% of the total number of reactions followed by $(\gamma, 3n)$, $(\gamma, 5n)$, and $(\gamma, 2n)$ with 4.8, 0.10, and 0.01%, respectively. The average neutron energy decreases with increasing neutron index i ($i = 1, 2, \ldots, x$) in each (γ, xn) reaction. As indicated in the figure, the average energy amounts to the highest value

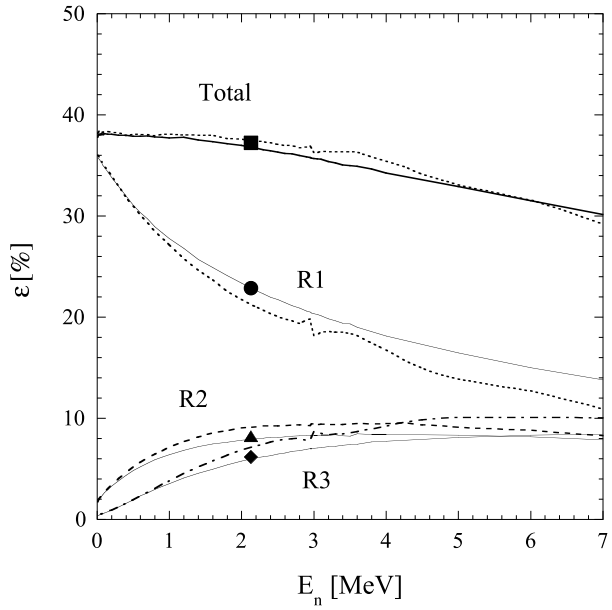

Fig. 3. The total detection efficiency and efficiencies of the individual rings of the flat-response neutron detector. Results of the calibration with a ^{252}Cf source are shown by the filled symbols. Results of the MCNP Monte Carlo simulations for monochromatic neutrons are shown by the broken lines, while those for the neutron-evaporation spectra by the solid lines.

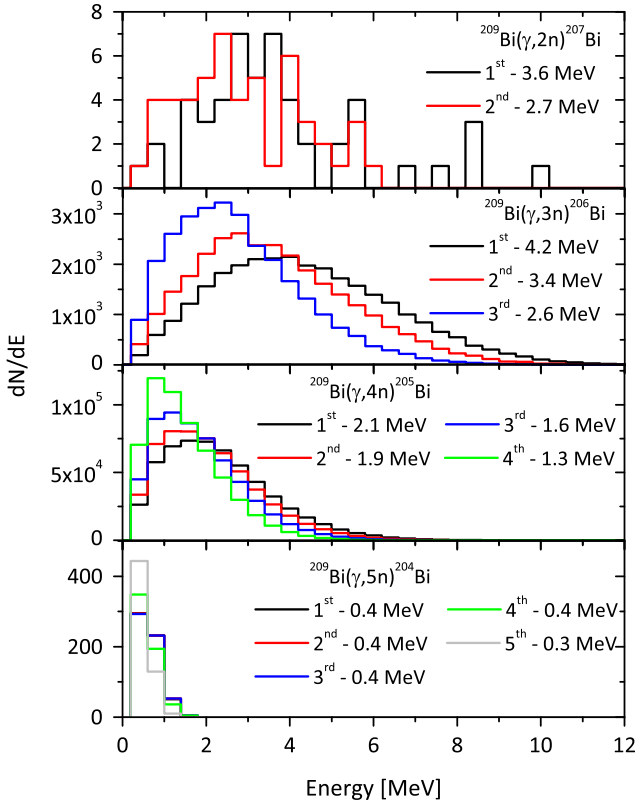

Fig. 4. (Color online) Results of the Monte Carlo statistical model calculations of neutron energy spectra in the ^{209}Bi(γ, xn) reaction at 40 MeV.

4.2 MeV for the first neutron emission in the $(\gamma, 3n)$ reaction. Thus, the flat response up to 5 MeV may suffice to the present neutron-multiplicity sorting.

Photoexcitation of nuclei is governed by the leading multipolarity 1. We previously investigated s- and p-wave neutron emissions following E1 and M1 excitations of ^{208,207}Pb [19]. The emission of neutrons with

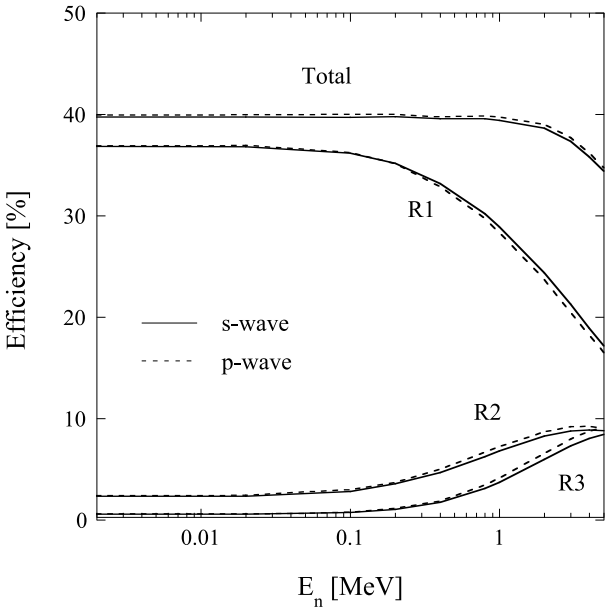

Fig. 5. MCNP Monte Carlo simulations of the detection efficiency of the flat-response neutron detector for s-wave (solid lines) and p-wave (dotted lines) neutrons.

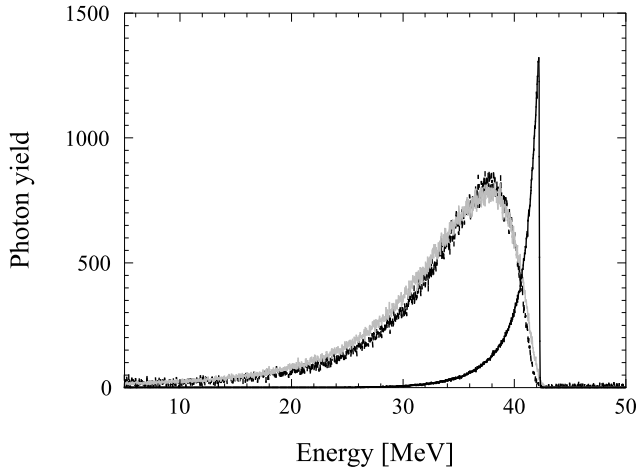

Fig. 6. Experimental response function of a $3.5'' \times 4.0''$ $LaBr_3$ (Ce) detector to a 42 MeV LCS γ-ray beam. A best fit to the experimental response function by the GEANT4 Monte Carlo simulation (gray line) and the resultant energy spectrum of the incident LCS γ-ray beam are also shown.

higher-partial waves are considerably suppressed by the centrifugal potential. γ-ray beams produced in laser Compton scattering in the head-on collision geometry keep linear polarization of laser photons and thus are linearly polarized nearly 100%. Obviously s-wave neutrons are emitted isotropically. In contrast, taking the x-axis along the vertical polarization defined by the electric component of the electromagnetic wave and the z-axis along the γ-ray beam, the angular distribution of p-wave neutrons is expressed [20] by

$$W(\theta,\phi) = \frac{3}{8\pi}[\sin^2\theta(1+\cos 2\phi)], \tag{6}$$

where θ stands for the polar angle and ϕ the azimuthal angle.

We simulated the detection efficiency of the FED for evaporation spectra of s- and p-wave neutrons with the GEANT4 code. Fig. 5 shows results of the simulation. One can see that the FED has nearly identical efficiencies for s- and p-wave neutrons, where the strong spatial anisotropy in the p-wave neutron emission is smeared out during the thermalization of neutrons in the moderator. The smearing effect was also confirmed for our high-efficiency neutron detector with 20 ^{3}He counters [21]. This is a common feature of moderation-based neutron detectors of the Livermore type.

It is to be noted that the MCNP (Fig. 3) and GEANT4 (Fig. 5) codes give detection efficiencies that are different by less than 2 percent. This may be attributed to nuclear data for neutron interactions used in the two codes.

3. Key experimental elements

We have begun experiments to provide (γ, xn) cross sections for the IAEA-CRP based on the present methodology of direct neutron multiplicity sorting at the NewSUBARU synchrotron radiation facility. In this section, we discuss key experimental elements.

3.1. Laser compton scattering γ-ray beams

γ-ray beams are produced in the Compton scattering of laser photons from relativistic electrons circulating in the NewSUBARU storage ring. The laser Compton scattering (LCS) converts a laser beam to a quasi-monochromatic γ-ray beam with an energy-amplification factor, $\sim 4\gamma^2$, where γ is the Lorentz factor, $\gamma = E_e/mc^2$. The Lorentz factor is about 2000 at the electron energy E_e =1 GeV. Thus, the amplification factor is 16 million, producing a 32 MeV γ-ray beam from a 2 eV ($\lambda \sim 532$ nm) photon beam. The LCS γ-ray beam, whose energy varies with the square of the electron energy, is energy-tunable from 8 to 76 MeV with the use of the 532 nm photons at NewSUBARU where the electron beam energy can be changed from 0.5 to 1.5 GeV.

3.1.1. Laser frequency

Q-switch lasers at a typical frequency 1 kHz are needed to produce pulsed LCS γ-ray beams in direct neutron-multiplicity sorting with a slow moderator-based neutron detector. We used a Pockels Cell to reduce the minimum frequency (16 kHz) of the INAZUMA (Nd:YVO_4) laser in the initial stage, which is now replaced with the Talon laser (λ =532 nm) which can be operated at 1 kHz.

3.1.2. Energy profile of γ-ray beams

The LCS γ-ray beam is quasi-monochromatic with energy spreads essentially determined by the electron beam emittance and the size of the collimator. The energy profile of the LCS γ-ray beam can be determined by means of Monte Carlo simulations of response functions of a $LaBr_3$ (Ce) detector to the γ-ray beams. For this purpose, a GEANT4 code that has incorporated the kinematics of the laser Compton scattering was developed. The electron beam energy has been calibrated with the accuracy of the order of 10^{-5} [22]. The energy is reproduced in every injection of an electron beam from a linear accelerator to the NewSUBARU storage ring at the nominal energy 974 MeV. The reproducibility of the electron energy is assured in the deceleration down to 0.5 GeV and acceleration up to 1.5 GeV by an automated control of the electron beam-optics parameters.

Fig. 6 shows a response function of a $3.5'' \times 4.0''$ $LaBr_3$ (Ce) detector to a 42 MeV LCS γ-ray beam. The energy distribution of the incident LCS γ-ray beam which leads to a best fit to the response function in interactions with the $LaBr_3$ (Ce) detector is also shown in the figure. The LCS γ-ray beam is virtually background-free. The synchrotron radiation and natural background γ-rays stay in the low-energy region. This is in contrast to the fact that γ-ray beams produced by the positron annihilation in flight were accompanied by background γ-rays generated by the positron bremsstrahlung [3].

3.2. Flux of γ-ray beams

The number of γ-rays incident on a target nucleus needs to be determined accurately in order to obtain absolute cross sections. A pulsed γ-ray beam is produced in collisions between laser photons and

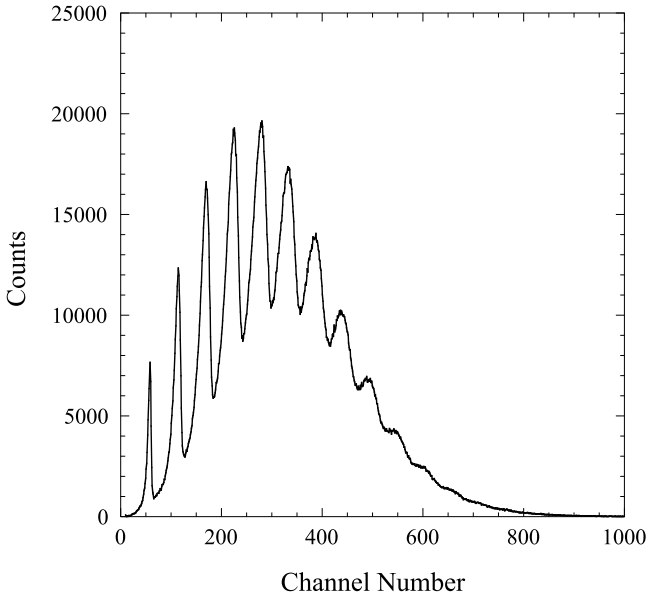

Fig. 7. Multi-photons spectrum of a 17 MeV LCS γ-ray beam measured with an $8.0'' \times 12.0''$ NaI(Tl) detector.

relativistic electrons. The laser pulse width is 60 ns for the INAZUMA laser and 25–40 ns for the Talon laser. The frequency and pulse width of the electron beam are 500 MHz and 60 ps, respectively. Thus, the time profile (width and frequency) of the LCS γ-ray beam is the same as that of the laser. Under the condition that large numbers of photons and electrons collide with small collision probability, the number of γ quanta involved in single γ pulse follows the Poisson distribution [23,24]. The number of γ-rays is determined from multi-photon spectra that are characterized by the Poisson distribution with an experimental formula given in Ref. [25]. An $8.0'' \times 12.0''$ NaI(Tl) detector with 100% detection efficiency is used as a flux monitor of the LCS γ-ray beam. Fig. 7 shows a multi-photon spectrum of a 17 MeV LCS γ-ray beam.

3.3. Neutron arrival-time distributions

The most essential information in the present direct neutron-multiplicity sorting is neutron arrival-time distribution. Neutrons produced in the (γ, xn) reaction are detected event-by-event with the moderation-based flat-efficiency detector during the γ pulse interval which is typically 1ms. We record arrival times for the first-, second-, third-arriving neutrons, etc. Note that the arrival time corresponds to the order of neutron detection governed by the slow moderation process, not to the order of neutron emission in the (γ, xn) reaction.

3.3.1. Characteristics of arrival times

Fig. 8 shows arrival-time distributions for single (Fig. 8(a)) and double (Fig. 8(b)) neutron events observed in the ^{197}Au(γ, xn) reaction at 17 MeV which lies between the two- and three-neutron separation energies, 14.7 MeV and 23.1 MeV, respectively. One can easily identify single neutron events on top of the background events in Fig. 8(a). For double neutron events, one can see the first-and second-arriving neutrons as well as the sum of them in Fig. 8(b). The arrival-time distribution for both single and double sum events is well characterized by a linear combination of two exponential functions, $T(t) = a \cdot \exp(-(t - t_0)/\tau_1) + b \cdot \exp(-(t - t_0)/\tau_2)$ with time constants (τ_1 and τ_2) and an offset time (t_0). The best fits are shown by the red lines. The time constants are nearly identical for both single and double sum events, $\tau_1 \sim 10$ μs and $\tau_2 \sim 100$ μs, which is natural because two neutrons are emitted in the ^{197}Au$(\gamma, 2n)$ reaction nearly simultaneously compared to the time needed for moderation and are detected without identifying

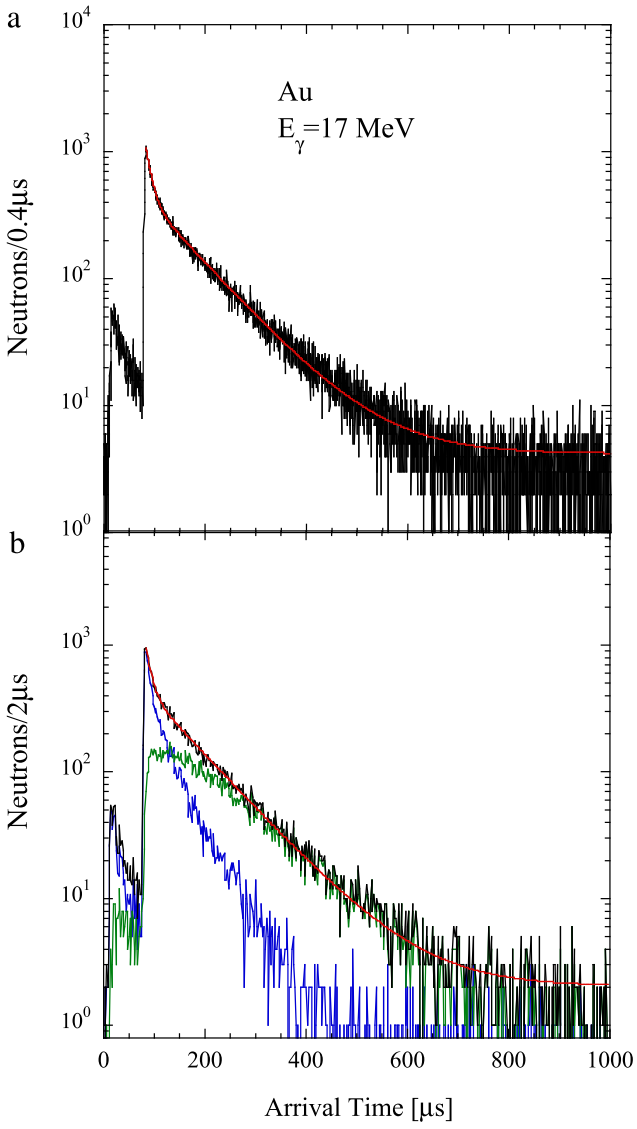

Fig. 8. (Color online) Arrival-time distributions of neutrons for the single neutron events (a) and double neutron events (b) in the ^{197}Au(γ, xn) reaction at 17 MeV. For the double neutron events, the arrival-time distribution is shown for the 1st- (blue) and 2nd-arriving (green) neutrons as well as the sum neutrons. The best fits to the single neutron events (a) and double sum neutron events (b) shown by the red lines were obtained with (a) $\tau_1 = 10.8 \pm 0.1$ and $\tau_2 = 99.6 \pm 0.6$ and (b) $\tau_1 = 11.5 \pm 0.3$ and $\tau_2 = 103.3 \pm 1.1$, respectively.

the order of detection. In contrast, when the order of detection is identified, one can see different arrival-time distributions in Fig. 8(b); the 1st-arriving neutrons are pushed to early times by the 2nd-arriving neutrons.

Note that there is a tiny contribution from a pre-pulse that is ahead of the main pulse by 66.7 μs corresponding to the frequency of the E-pulse (15 kHz) whose function is to maintain a constant pulse energy. The pre-pulse is generated by an energy release in the first pulse suppression mode of the Talon operation whenever the operating frequency (1 kHz) is less than the E-pulse frequency.

Fig. 9 shows arrival-time distributions for single (Fig. 9(a)), double (Fig. 9(b)), and triple (Fig. 9(c)) neutron events observed in the ^{209}Bi(γ, xn) reaction at 34 MeV which lies above the four-neutron separation energy at 29.5 MeV. The data were acquired in the top-up operation of the NewSUBARU electron storage ring. The electron beam current of the storage ring was kept constant at 200 mA in the top-up operation by automatic injections of 974 MeV electrons from

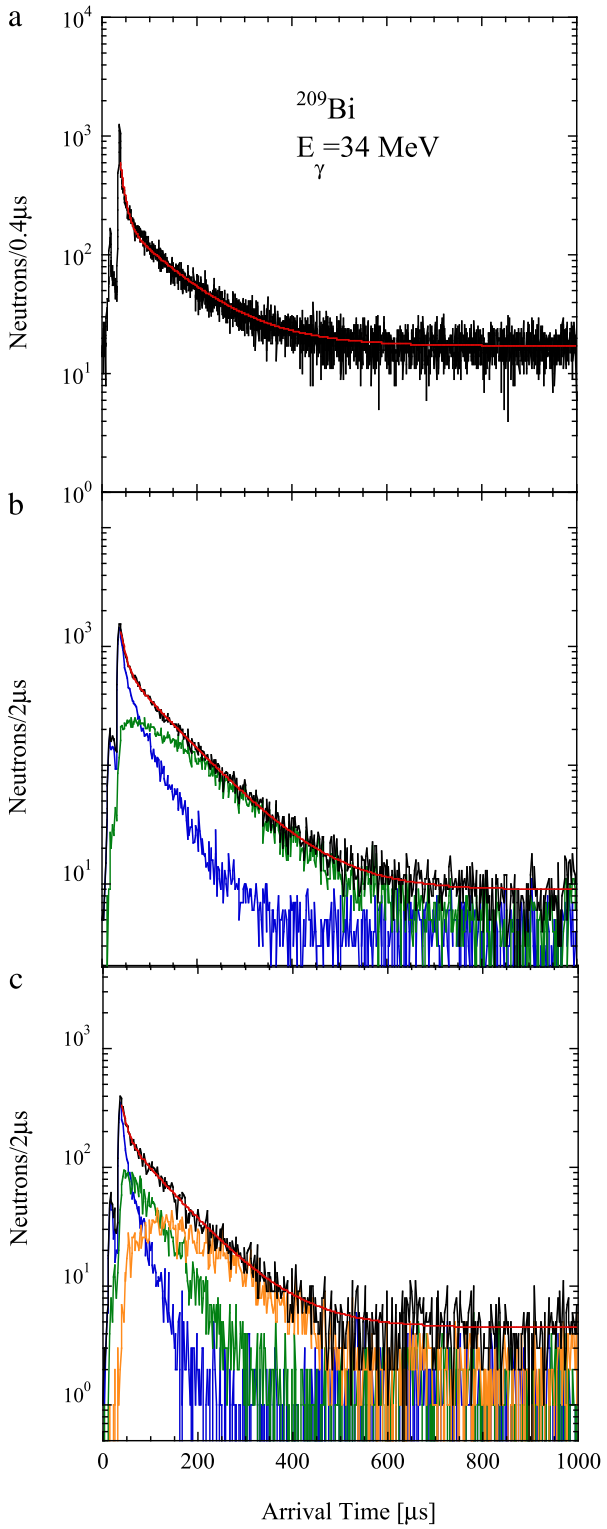

Fig. 9. (Color online) Arrival-time distributions of neutrons for the single neutron events (a), double neutron events (b), and triple neutron events (c) in the ^{209}Bi(γ, xn) reaction at 34 MeV. For the double neutron events, the arrival-time distribution is shown for the 1st- (blue) and 2nd-arriving (green) neutrons as well as the sum neutrons. Similarly, for the triple neutron events, the arrival-time distribution is shown for the 1st- (blue), 2nd- (green), and 3rd-arriving (orange) neutrons as well as the sum neutrons. The best fits to the single (a), double sum (b), and triple sum events (c) are shown by the red lines.

the electron linear accelerator. One can see relatively high background neutrons in the single events shown in Fig. 9(a). The background neutrons were generated upstream of the γ-ray beam line at the time of the automatic injection. The single, double- and triple-sum events are again characterized by essentially the same time constants of 10 and 100 μs as shown by the red lines in Fig. 9(a), (b), and (c). One can see that the 1st- and 2nd-arriving neutrons of the triple neutron events are further pushed to earlier times by the 3rd-arriving neutrons (Fig. 9(c)) compared to those of the double neutron events (Fig. 9(b)).

3.3.2. *Remarks on random coincidences and multiple firings*

The ratios of background neutrons to reaction neutrons in single neutron events of Figs. 8(a) and 9(a) are 1/17.0 and 1/1.55, respectively. Background neutrons may cause random coincidences with reaction neutrons to generate double, triple neutron events etc.

The neutron count-rate was 32.1cps in the ^{197}Au(γ, xn) reaction at 17 MeV and 8.4cps in the ^{209}Bi(γ, xn) reaction at 34 MeV. Multiple firings of (γ, n) reactions by a single pulse of the LCS γ-ray beam may also contribute to double, triple neutron events etc.

The random coincidences and multiple firings may need to be considered in the data reduction to accurately determine partial photoneutron cross sections. These effects will be reported in forthcoming papers on individual measurements based on the present experimental methodology.

4. Summary

Pioneering works at Livermore in the 20th century with moderation-based neutron detectors and in-flight positron-annihilation γ-ray beams have greatly contributed to our understanding of nuclear responses to the isovector giant dipole resonance. Now we are entering into a new era of GDR studies with a mission of the IAEA-CRP to resolve the long-standing discrepancy between the Livermore and Saclay data of partial photoneutron cross sections. We have developed a flat-efficiency neutron detector for the mission that enables us to directly sort the neutron-multiplicity without relying on the ring-ratio technique. In this paper, we discussed the methodology of the direct neutron-multiplicity sorting to determine (γ, xn) cross sections along with key experimental elements including the frequency, energy-profile and flux of the laser Compton scattering γ-ray beam. The methodology has so far been used to measure (γ, xn) cross sections for ^{209}Bi, ^{197}Au, ^{169}Tm, ^{89}Y, and ^{9}Be. Results of those measurements will be reported separately in forthcoming papers.

Acknowledgments

This work was supported by the IAEA under the contract numbers for the CRP-F41032, JPN-20564, ROM-20476, and RUS-20501 and by the Konan University as the Premier Project. We are grateful to Hideaki Ohgaki of the Institute of Advanced Energy of Kyoto University for making a 3.5″ × 4.0″ $LaBr_3$(Ce) detector available to the PHOENIX Collaboration of the Premier Project. I.G. and D.F. acknowledge the support from the Extreme Light Infrastructure Nuclear Physics (ELI-NP) Phase II, a project co-financed by the Romanian Government and the European Union through the European Regional Development Fund—the Competitiveness Operational Programme (1/07.07.2016, COP, ID 1334).

References

[1] B.L. Berman, S.C. Fultz, Measurements of the giant dipole resonance with monoenergetic photons, Rev. Modern Phys. 47 (1975) 713–761.
[2] S.S. Dietrich, B.L. Berman, Atlas of photoneutron cross sections obtained with monoenergetic photons, At. Data Nucl. Data Tables 38 (1988) 199–338.
[3] Handbook on photonuclear data for applications - Cross-sections and spectra, IAEA-TECDOC-1178 IAEA, October, 2000.
[4] V.V. Varlamov, B.S. Ishkhanov, Giant dipole resonance in photonuclear experiments of various types: Discrepancies, reasons, methods of overcoming, and consequences, Phys. Part. Nucl. 35 (2004) 459.
[5] V.V. Varlamov, B.S. Ishkhanov, V.N. Orlin, New approach to analyzing and evaluating cross sections for partial photoneutron reactions, Phys. Atomic Nuclei 75 (2012) 1339.

[6] V.V. Varlamov, B.S. Ishkhanov, V.N. Orlin, K.A. Stopani, A new approach for analysis and evaluation of partial photoneutron reaction cross sections, Eur. Phys. J. A 50 (2014) 114.
[7] B.S. Ishkhanov, V.N. Orlin, V.V. Varlamov, Total and partial photoneutron reactions cross sections - new analysis and evaluation, EPJ Web. Conf. 38 (2012) 12003.
[8] B.S. Ishkhanov, V.N. Orlin, N.N. Peskov, V.V. Varlamov, Photoneutron reactions in the range of giant dipole resonance, Phys. Part. Nucl. 48 (2017) 76.
[9] H. Beil, R. Bergere, A. Veyssiere, Systeme de detection de photoneutrons utilisant un scintillateur a grandes dimensions permettant l'etude simultanee des reactions (γ, xn), Nucl. Instrum. Methods 67 (1969) 293.
[10] S.C. Fultz, et al., Photoneutron cross-section measurements on gold using nearly monochromatic photons, Phys. Rev. 127 (1962) 1273.
[11] B.L. Berman, et al., Photoneutron cross sections for Zr^{90}, Zr^{91}, Zr^{92}, Zr^{94}, and Y^{89}, Phys. Rev. 162 (1967) 1098.
[12] M.A. Kelly, et al., Effect of nuclear polarization on the giant dipole resonance of Ho^{165}, Phys. Rev. 179 (1969) 1194.
[13] L.V. East, R.B. Walton, Polyethylene moderated ^{3}He neutron detectors, Nucl. Instrum. Methods 72 (1969) 161.
[14] H. Utsunomiya, et al., Photodisintegration of ^{9}Be through the $1/2^{+}$ state and cluster dipole resonance, Phys. Rev. C 92 (2015) 064323.
[15] J.F. Briesmeister, computer code MCNP, Version 4c, (Los Alamos National Laboratory, Las Alamos, 2000).
[16] Properties of Neutron Sources, IAEA-TECDOC-410 IAEA, March, 1987.
[17] V.F. Weisskopf, Statistics and nuclear reactions, Phys. Rev. 52 (1937) 295.
[18] T. Kawano, (Private communication).
[19] T. Kondo, et al., Total and partial photoneutron cross sections for Pb isotopes, Phys. Rev. C 86 (2012) 014316.
[20] J.M. Blatt, V.F. Weisskopf, Theoretical Nuclear Physics, Springer-Verlag, New York Inc., 1979, p. 593.
[21] F. Camera, et al., Gamma above the neutron threshold experiments at ELI-NP, Rom. Rep. Phys. Supplement 68 (2016) S539.
[22] H. Utsunomiya, et al., Energy calibration of the NewSUBARU storage ring for laser Compton-scattering gamma rays and applications, IEEE Trans. Nucl. Sci. 61 (2014) 1252.
[23] T. Kii, et al., Photon counting method for high flux pulsed laser-Compton backscattered photons based on Poisson model, in: Proceedings of the 12th Symposium on Accelerator Science and Technology, ed. Yasushige Yano (The Institute of Physical and Chemical Research (RIKEN)), Wako, Japan, 1999, pp. 484.
[24] H. Toyokawa, et al., Flux measurement of the laser-Compton-backscattered photons with a Poisson fitting method, IEEE Trans. Nucl. Sci. 47 (2000) 1954.
[25] T. Kondo, et al., Determination of the number of pulsed laser-Compton scattering photons, Nucl. Instrum. Methods A 659 (2011) 462.